NeuroImage: Clinical 6 (2014) 64–76

Contents lists available at ScienceDirect

NeuroImage: Clinical

journal homepage: www.elsevier.com/locate/ynicl

Localizing ECoG electrodes on the cortical anatomy without post-implantation imaging

Disha Gupta[a,b,c,*], N. Jeremy Hill[b,d], Matthew A. Adamo[e], Anthony Ritaccio[a], Gerwin Schalk[a,b,f,g,h,i]

[a]Dept. of Neurology, Albany Medical College, Albany, NY, USA
[b]Neural Injury and Repair, Wadsworth Center, New York State Dept. of Health, Albany, NY, USA
[c]Early Brain Injury and Motor Recovery Lab, Burke-Cornell Medical Research Institute, White Plains, NY, USA
[d]Translational Neurological Research Laboratory, Helen Hayes Hospital, West Haverstraw, NY, USA
[e]Dept. of Neurosurgery, Albany Medical Center, Albany, NY, USA
[f]Dept. of Neurosurgery, Washington University, St. Louis, MO, USA
[g]Dept. of Biomed. Eng., Rensselaer Polytechnic Institute, Troy, NY, USA
[h]Dept. of Biomed. Sci., State Univ. of New York at Albany, Albany, NY, USA
[i]Dept. of Elec. and Comp. Eng., Univ. of Texas at El Paso, El Paso, TX, USA

ARTICLE INFO

Article history:
Received 20 June 2014
Received in revised form 26 July 2014
Accepted 29 July 2014
Available online 21 August 2014

Keywords:
Electrocorticography (ECoG)
Electrode localization
Fiducials
Auditory processing
interaoperative localization

ABSTRACT

Introduction: Electrocorticographic (ECoG) grids are placed subdurally on the cortex in people undergoing cortical resection to delineate eloquent cortex. ECoG signals have high spatial and temporal resolution and thus can be valuable for neuroscientific research. The value of these data is highest when they can be related to the cortical anatomy. Existing methods that establish this relationship rely either on post-implantation imaging using computed tomography (CT), magnetic resonance imaging (MRI) or X-Rays, or on intra-operative photographs. For research purposes, it is desirable to localize ECoG electrodes on the brain anatomy even when post-operative imaging is not available or when intra-operative photographs do not readily identify anatomical landmarks.
Methods: We developed a method to co-register ECoG electrodes to the underlying cortical anatomy using only a pre-operative MRI, a clinical neuronavigation device (such as BrainLab VectorVision), and fiducial markers. To validate our technique, we compared our results to data collected from six subjects who also had post-grid implantation imaging available. We compared the electrode coordinates obtained by our fiducial-based method to those obtained using existing methods, which are based on co-registering pre- and post-grid implantation images.
Results: Our fiducial-based method agreed with the MRI–CT method to within an average of 8.24 mm (mean, median = 7.10 mm) across 6 subjects in 3 dimensions. It showed an average discrepancy of 2.7 mm when compared to the results of the intra-operative photograph method in a 2D coordinate system. As this method does not require post-operative imaging such as CTs, our technique should prove useful for research in intra-operative single-stage surgery scenarios.
To demonstrate the use of our method, we applied our method during real-time mapping of eloquent cortex during a single-stage surgery. The results demonstrated that our method can be applied intra-operatively in the absence of post-operative imaging to acquire ECoG signals that can be valuable for neuroscientific investigations.

1. Introduction

Electrocorticographic (ECoG) signals are captured by electrode arrays that are implanted directly on the surface of the brain. ECoG grids are implanted in 20–40% of resection surgeries for brain disorders such as epilepsy and tumors, and used to delineate eloquent cortex (Yuan et al., 2012). They are also used in longer-term monitoring protocols to localize seizure foci. Over the past decade, an increasing number of studies have begun to explore the value of ECoG for neuroscientific research (Chang et al., 2010; Crone et al., 2001, 2006; Flinker et al., 2010; Gunduz et al., 2012; Hill et al., 2012; Kubanek et al., 2009; Miller et al., 2007a; Pei et al., 2011; Schalk et al., 2007; Sinai et al., 2005, 2009). In both clinical and research applications, the significance of ECoG data is highest when the electrode locations can be related to the cortical anatomy. This relationship can be established using pre- and post-operative imaging in two-stage surgeries, as performed for pre-surgical evaluation for epilepsy resections, where a grid of electrodes is implanted on the cortex in the first surgery and is removed

* Corresponding author at: Burke-Cornell Medical Research Institute, Sturgis Bld, Suite M109, White Plains, NY, USA.
E-mail address: dig2015@med.cornell.edu (D. Gupta).

http://dx.doi.org/10.1016/j.nicl.2014.07.015

in the second surgery after a monitoring period of several days. Common techniques to do this include (a) co-registering a pre-operative MRI with a post-operative CT with (Dykstra et al., 2012; Hermes et al., 2010) and without a correction for brain-shift (Grzeszczuk et al., 1992; Sebastiano et al., 2006; Tao et al., 2009; Winkler et al., 2000); (b) co-registering a pre-operative MRI with a post-operative MRI (Kovalev et al., 2005; Yang et al., 2012); (c) co-registering a pre-operative MRI with a post-operative X-Ray (Miller et al., 2007b); and (d) estimating electrode positions directly from a post-operative MRI via curvilinear reformatting (Schulze-Bonhage et al., 2002).

These methods have proven to be valuable, but are entirely dependent on post-operative imaging. Moreover, in contrast to the typical ECoG grids whose electrode disks are placed 10 mm apart, high-density grids with denser packing of electrodes (inter-electrode distance of <5 mm) are increasingly being explored for improved clinical monitoring and neuroscientific research (Kellis et al., 2010; Van Gompel et al., 2008). Current post-operative imaging systems are typically unable to resolve individual electrodes from such densely packed arrays. Most importantly, post-operative imaging may simply be unavailable. It may be contraindicated for clinical reasons, it may be rendered useless for localization due to artifacts (Silberbusch et al., 1998), or it may be irrelevant because the surgery in question is a single-stage procedure during which the grid is placed only temporarily and removed before closing.

Alternatively, some studies have used intra-operative photographs together with pre-operative imaging, with or without post-operative imaging (Dalal et al., 2008; Wellmer et al., 2002). However, the procedure relies on the visibility and access to prominent sulcal patterns (vascular landmarks) in the pre-operative photographs as well the MRI. However, in either case, co-registration with photographs is limited by good visibility of such anatomical landmarks through the grid. As electrode density increases, the visibility of the cortex through the grid decreases. Sometimes, the area being operated does not have prominent identifiable vascular or sulcal structures, such as in the frontal cortex as opposed to the temporal cortex. Previous surgeries with cortical resection may also distort the sulcal patterns, making it challenging to identify them on both the photograph and the MRI clearly. Moreover, intra-operative bleeding may obstruct the view through the grid. Thus, acquiring electrode locations for ECoG research without intra- and post-operative imaging, in single- or two-stage operations, remains an unmet gap.

Thus, acquiring electrode locations for ECoG research without intra- and post-operative imaging, in single- or two-stage operations, remains an unmet gap. Our study aims to demonstrate a link between existing engineering methods and existing clinical tools that can be used to fill this gap. Specifically, our first aim was to demonstrate the procedural combination of methods that are feasible and practical for application in ECoG research scenarios. Our second aim was to determine the practical utility of this method (e.g., as assessed by localization error) compared to existing methods that are commonly used for ECoG research. Our third aim was to assess the impact of specific parameters (such as fiducial placement and number), and to quantify these in a systematic ECoG human study in a real-world situation.

We describe a method that can be used to localize ECoG electrodes on the cortical anatomy during single-stage procedures without requiring post-operative imaging or intra-operative photographs. Our method depends on fiducials that allow to co-register the external coordinate space of the surgery (where the grid is physically located on the cortex) to the coordinate space in which a 3D cortical model is rendered from the pre-operative MRI. A similar procedure is performed by various neuronavigator systems such as the BrainLab VectorVision (BrainLab AG, Feldkirchen, Germany) or the Medtronics StealthStation (Medtronic Inc., Minneapolis MN, USA). However, these clinical stereotactic devices may export locations in a different coordinate system from that of the images used for research. To account for this difference, our method includes a step in which we estimate the rotation and translation of these two coordinate systems. In sum, our approach can localize electrodes on the cortical anatomy using pre-operative MRIs and intra-operative use of a neuronavigation device. Thus, our approach greatly facilitates ECoG research studies with patients who undergo single-stage surgical procedures such as tumor resections, thereby allowing access to a more variable and much larger subject population than those that receive pre-operative and post-operative imaging (i.e. typically patients with epilepsy). Furthermore, it has the additional benefit of allowing the estimation of grid shifts from the time of grid placement to subsequent monitoring. This is important, because a previous report (LaViolette et al., 2011) has reported grid shifts by as much as 7 mm.

We validate our procedure by applying it to data from two-stage procedures and comparing its results with the outcome of two conventional methods: one that relies on post-operative imaging and another that uses intra-operative photographs.

It should be noted that the resulting validation metric ('error') is not, strictly speaking, an error measure attributable to a single method, but rather a *discrepancy between the results of two methods*, of which the relative contributions of the two methods are unknown. Thus, this measure almost certainly reflects an overly pessimistic report of our method, but in the absence of any other gold-standard measures for validation, it is the first step towards assessing this method. Another possible route to validating our localization method would be to assess the functional and anatomical concordance of the signals acquired from these intra-operatively localized electrodes. We demonstrate one such application in the last section, in which we demonstrate the co-registration of a high-density ECoG micro-grid.

2. Methods

2.1. Localization procedure

2.1.1. Overview

To localize electrodes on a 3-D rendering of the cortical surface, we must map the three-dimensional coordinate system of the physical space in which the surgery is performed to an imaging coordinate system in which cortical structural information is available. Neurosurgeons routinely do this using frameless stereotactic neuronavigation systems such as BrainLab VectorVision or Medtronics StealthStation. These systems allow intra-operative navigation and localization of the human cortical structures, have been extensively studied, and are approved for clinical use. They have the capability to create a reference frame in the external surgical coordinate system Ω_S and acquire coordinates of points in that system. They then transform these coordinates to an internal imaging coordinate system, which we will call Ω_P, such that these points can now be projected on to a 3-dimensional cortical model obtained from pre-operative imaging scans. Once the patient's head has been fixed and its position registered with the system, the neuronavigator can display the position of the surgical instrument relative to the brain images in Ω_P in real time.

The cortical model may not be made directly available to researchers by the neuronavigation system. Researchers must typically use additional software, such as CURRY (Compumedics, Charlotte, NC, USA) or SPM (Wellcome Trust Centre for Neuroimaging, University College London) to create a 3D rendering of the cortical surface from the imaging data in their own coordinate system Ω_Q. Unfortunately, the Ω_P and Ω_Q are not necessarily (and typically are not) identical. This is because the image selected for modeling in Ω_Q (usually a pre-operative MRI) will often be only one of multiple imaging modalities that are combined together in the neuronavigator. Specifically, the surgeon may require the neuronavigator to combine CT, PET and functional MRI images, as well as structural MRIs taken with multiple contrast and weighting methods, all of which are taken at different times at slightly different angles. The neuronavigator interfaces are usually simplified, so that the details of the precise transformations between these different imaging spaces are not accessible or configurable. In practice, this means that

the coordinates available to us in Ω_P may be defined along axes that are arbitrarily rotated and translated relative to those of Ω_Q.

The estimation of a rigid-body transform from one space to another is called *co-registration* of the coordinate systems. We use a point-based co-registration approach, as this has been found to be quick and reliable and is most commonly used among the various co-registration methods (West et al., 1996). In point-based co-registration, a set of corresponding points, called *fiducials*, are identified separately in each of the two coordinate systems. These two sets of corresponding 3-dimensional coordinates are used to determine the parameters of rotation, translation and scaling transformations that can optimally align them. These transformations can then be used to transform novel points acquired in the first coordinate system into the second coordinate systems, always maintaining their relative spatial relationships.

A pre-requisite for our procedure is the ability to record coordinates of arbitrary points from the neuronavigator and to retrieve their numerical values afterwards. Methods for doing so vary according to the model and version of the neuronavigation system. It may also be possible to create a formal link between the neuronavigator and an external computer, as with BrainLab's *VectorVision Link* product. Alternatively, if the neuronavigator screen reports coordinates explicitly, they may be noted down by hand. Our research was conducted without VectorVision Link and without the function of seeing the numerical coordinates on the screen. However, our version of the basic VectorVision system allowed access to coordinates in Ω_P via two plain text files, `Logfile.txt` and `Pointfile.txt`. These were deleted on shutdown but could be preserved by saving the system's current data to a memory stick or DVD before shutting down.

Our procedure can be summarized as follows:

Before the surgery:

2.1.2 Obtain pre-operative MRI.

2.1.3 If the pre-operative MRI does not have fiducial markers, obtain a pre-operative CT with fiducial markers.

During the surgery:

2.1.4 Register the surgical space to the neuronavigator.

2.1.5 Obtain neuronavigator coordinates for the fiducial markers.

2.1.6 Obtain neuronavigator coordinates for the target electrode locations.

After the surgery:

2.1.7 Acquire final coordinates for the fiducial markers using the neuroimaging research software.

2.1.8 Estimate the transformation from the neuronavigator system to the final coordinate system.

2.1.9 Transform the target electrode locations to the final space.

2.1.10 Interpolate and project the remaining electrode positions.

These 9 steps are explained in greater detail in the following subsections (Fig. 1).

2.1.2. Pre-operative MRI

To extract the anatomical structure and render the subject-specific 3D cortical surface, a high resolution pre-operative MRI is necessary. We acquire T1-weighted, sagittal 3D spoiled gradient echo (SPGR) MRI images with a 1.5 T or (preferably) 3 T machine. The MRI is obtained for the entire brain, using a slice width of 1 mm, with the subject held in a fixed position relative to the imaging system.

2.1.3. Fiducials

Point-based co-registration requires three or more non-collinear stationary points that are identifiable in both of the spaces to be co-registered. Errors in acquiring the precise locations of these *fiducial* locations in the two coordinate systems will result in localization errors for all points of interest. Fiducial localization errors can be detected and quantified as discussed in Section 2.2.

It is sometimes possible to use salient anatomical features such as the nasion, inion, and left and right pre-auricular points, and left and right mastoids. However, since such landmarks can be localized only imprecisely in images, this method must be expected to yield larger co-registration errors than the use of special-purpose fiducial markers.

Fiducial markers are spherical capsules that are temporarily affixed to the body of the subject. They can be mounted on invasive screws that are secured to the skull, or on stick-on plates pasted on the skin. The capsule material is specific to the imaging modality, since it must be safe to use in the scanner, and clearly detectable in the images while causing minimal distortion. The markers show up as readily identifiable high-contrast dots in the image data. The size of the fiducial markers should be slightly larger than the dimension of an imaging voxel, so that the center of the marker is accurately detected and resolved from the scanned images.

Fiducial markers are used in our procedure both for neuronavigator registration (i.e. co-registration of Ω_S with Ω_P) and for image alignment (co-registration of Ω_P with Ω_Q). Although alternative methods exist for neuronavigator registration, the use of fiducial markers is expected (according to the BrainLab VectorVision manual) to yield the most accurate results, according to both our edition of the BrainLab VectorVision manual and a study by Woerdeman et al. (2007) using the StealthStation.

The fiducial locations should be well distributed such that they cover the front, back, top, and both sides of the head, and placed such that there is variation in the distances between them (Wang and Song, 2010). The absolute minimum number of fiducial points is 3, but it is beneficial to have a larger number, as we demonstrate in Section 3.

The fiducial markers must remain attached to the subject at the surgery onset. This necessitates that the pre-operative imaging be performed immediately prior to the surgery. For subjects where only an older pre-operative MRI (without fiducial markers) is available, and an in-house MRI will not be repeated on the day of surgery, fiducial marker positions may also be captured on a high-resolution CT (1 mm slice width, no angle, skin to skin).

2.1.4. Neuronavigator registration

The neuronavigator is a valuable tool for the surgeons in most of the surgeries that fall within the scope of our study. It is also useful for the researcher, since it acts as the transitional coordinate system that can record coordinates in a clinically approved manner, and later supply these to an external research system without compromising the clinical workflow.

Immediately prior to surgery, the neuronavigator must be set up with all the most up-to-date imaging data for the patient. First, the surgeon adds the various multimodal imaging datasets to the neuronavigator system. The most accurate co-registration results require end-to-end imaging data of good quality—i.e. high resolution, with minimal head movement and artifacts. Second, the navigator interface automatically detects any fiducial markers and extracts their centroid coordinates from the images. Errors can arise at this stage if the imaging data are of low resolution, due to inaccurate detection of the fiducial centroids. Third, the neuronavigator performs an automatic transformation of the multiple imaging datasets into a single coordinate system Ω_P using all the detected fiducials in combination with a surface or volume matching algorithm. Such co-registration of multimodal data has been shown to be source of an average error of approximately 2 mm (Mutic et al., 2001).

In the operating room, once the patient's head has been fixed in position for surgery, a frame of reference is established. This is performed by attaching a reference object to the clamp that holds the subject's head. The reference object in our study was a set of three passive reflective marker spheres positioned on three orthogonal axes, called a *reference star*. This star, which is part of the VectorVision system, reflects infra-red radiation emitted by the neuronavigator camera array. The

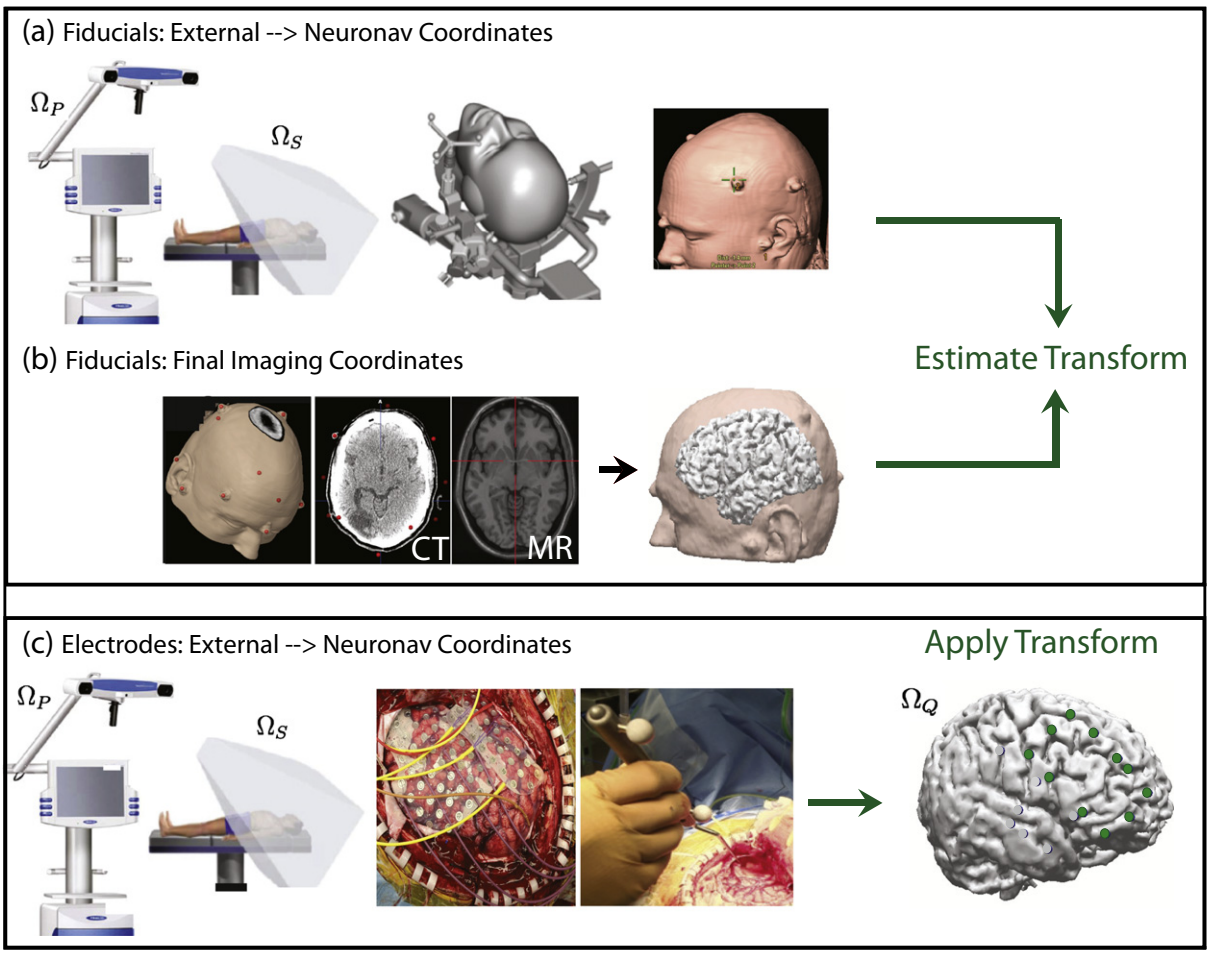

Fig. 1. The figure shows the steps for the fiducial-based intra-operative electrode localization and their validation. (a) The first step involves obtaining the *x*, *y* and *z* coordinates of the fiducials pasted on the subjects' scalp and face. This is performed with the help of a neuronavigator apparatus after the patient's head is fixed in the stereotaxic frame for the craniotomy. The neuronavigator is first registered to the physical space in which the subject is lying. Then the neuronavigator probe is placed on each fiducial to acquire the coordinates in the imaging space. (b) Next, the fiducial coordinates in the imaging space are acquired with the help of subject's pre-operative images such as MRI or CT (or co-registered CT and MRI) by detecting the visible fiducials. This is followed by the estimation of a transformation matrix between the physical space and the imaging space using (a) and (b). (c) Finally, to acquire the electrode locations of a grid placed on the cortex during the surgery, the neuronavigator probe is used to obtain the coordinates of the electrodes in the physical space. Applying the transformation matrix to these coordinates provides the electrode coordinates in the imaging space.

reflected beams are captured and digitized by two camera lenses. The navigator probe is similarly equipped with two reflective marker spheres, allowing the system to track its position and orientation in the space Ω_S defined by the reference, provided that the lines of sight from both camera lenses to the spheres on the reference star and probe are not obscured.

The neuronavigator must then be registered, i.e. it must perform the data-gathering and fitting operation that co-registers Ω_S with Ω_P. The first step is to touch the probe to the origin of the reference star.

Then, in fiducial-based neuronavigator registration, the neuronavigator prompts the surgeon to probe each of the fiducial locations in turn. The measured coordinates in Ω_S are used to estimate the transformation that maps them to the fiducial locations that were detected automatically in Ω_P during setup. The precision of neuronavigator co-registration has been extensively studied, and the typical fiducial registration error has been found to be 1.66 mm $\pm$ 0.61 mm (Kuehn et al., 2008).

Some neuronavigation systems have alternative methods for registration. The easiest method is to use a laser scanner that automatically samples three-dimensional coordinates of many points over bony surfaces such as the zygomatic bone, and sends them to the neuronavigator, which uses a surface-matching algorithm to co-register the points to Ω_P. However, we prefer to use fiducial markers where possible, since our equipment performs registration more accurately using markers: this has the collateral benefit of making fiducial marker positions available for the research method discussed in this paper.

2.1.5. Neuronavigator coordinates of fiducials

The mapping into the final research imaging space will require neuronavigator coordinates $\{\mathbf{p}_i\}$ for all the fiducial locations $i = 1 \ldots n$. If the fiducials themselves were used for registration, then the neuronavigator should already have a record of their coordinates. If another registration method was employed, then the neuronavigator probe must now be used to record coordinates for each of the fiducials in turn. Once these coordinates are obtained, the fiducial marker mounts can be removed from the subject's scalp, provided the reference star subsequently remains fixed relative to the head. If the head or the reference star is re-positioned before the target electrodes are localized, the fiducial coordinates must be re-acquired.

2.1.6. Neuronavigator coordinates of target electrodes

When the grid has been placed in its final position on the cortex, the neuronavigator probe is used to acquire coordinates in Ω_P for as many of the individual electrodes as possible. The neuronavigator registers all these 3-D coordinates relative to the reference star and transforms them into the Ω_P coordinate system. We note these coordinates by $\{\tilde{\mathbf{p}}_i\}$ for target locations $i = 1 \ldots m$.

To allow the remaining electrode positions from the entire grid to be interpolated as accurately as possible, the coordinate set should include points from widely spaced locations (e.g. as close to the corners and edges of the grid as possible) and these locations should not all be collinear. We acquire at least $m = 8$ electrode co-ordinates and more if possible. It is important to make a record of the electrode label or number that corresponds to each of the measured points in the correct chronological sequence (the neuronavigator's screenshot function may help with this).

2.1.7. Final coordinates of fiducials

The next step is to acquire coordinates for the fiducials by using neuroimaging software to locate them manually in the final imaging space Ω_Q, and to extract their 3-D coordinates $\{\mathbf{q}_i\}$ in the same order that their coordinates were acquired during surgery. If fiducial markers are not available directly in the pre-operative MRI, but rather in a separate pre-operative CT, then this step requires that the CT be co-registered to the MRI.

In our instantiation of this procedure, we used the CURRY software package to co-register a pre-operative CT with fiducial markers to the MRI. CT–MRI co-registration required manual identification of anatomical landmarks of nasion, inion, and pre-auricular points in both image datasets: these were used as a starting point for a landmark- and volume-based algorithm that computes the transformation for aligning the CT to the coordinate system of the MRI. This step itself, although more accurate than a procedure based on anatomical landmarks alone, can introduce errors: Ulin et al. (2010) report an average error of 2 mm in CT–MRI co-registration across 45 institutions and 11 software packages.

The procedure for manually acquiring the final fiducial coordinates was also carried out in CURRY.

2.1.8. Estimation of the rigid-body transform

The set of corresponding fiducial coordinates obtained from the neuronavigation imaging system Ω_P and the research imaging space Ω_Q are used to estimate a transformation matrix between these coordinate spaces using rigid-body transformation.

Let the two matched sets of n fiducial coordinates be $\{\mathbf{p}_i\}$ from Ω_P and $\{\mathbf{q}_i\}$ from Ω_Q, with the different fiducial locations being indexed by $i = 1, 2, \ldots, n$. Each $\mathbf{p}_i$ or $\mathbf{q}_i$ is a 3-element vector consisting of an x, a y and a z coordinate. We want to estimate the rigid-body transformation that rotates, scales and translates the $\mathbf{p}_i = [p_{xi}, p_{yi}, p_{zi}]^\top$ to align each one with the corresponding $\mathbf{q}_i = [q_{xi}, q_{yi}, q_{zi}]^\top$ in the Ω_Q, preserving all distances, maintaining the planarity of surfaces and the angles between them. This co-registration problem can be stated as follows:

$$\mathbf{q}_i = s\,\mathbf{R}\mathbf{p}_i + \mathbf{t},$$

where $\mathbf{R}$ is the 3×3 rotation matrix, s is the overall scaling factor, and $\mathbf{t}$ is the 3-element translation vector. The aim is to find the s, $\mathbf{R}$ and $\mathbf{t}$ that minimize the sum of squared distances between transformed matched pairs, such that the $\mathbf{R}$ remains a valid rotation matrix where $\mathbf{R}^\top\mathbf{R} = \mathbf{R}\mathbf{R}^\top = \mathbf{I}$, where $\mathbf{I}$ is the identity matrix. This problem of absolute orientation is usually solved by estimating the closest mapping in the least-squares sense in the 3 dimensions. There are many approaches, many of which use numerical methods to minimize residual errors iteratively. Most such methods only use 3 pairs of points to solve a set of linear equations, thereby neglecting the additional information provided by additional points. To reduce errors, we instead use Horn's unit quaternion method (Horn, 1987), which has two advantages: it can take advantage of the information in more than 3 points, and it is a closed-form solution that finds the global optimum and thus is not sensitive to initial configuration of the algorithm. This method has been found to be robust for 3D and 2D transformations for multiple points (Eggert et al., 1997). It is carried out by first constructing a positive symmetric matrix $\mathbf{N}$ as follows:

$$\mathbf{N} = \begin{bmatrix} (S_{xx}+S_{yy}+S_{zz}) & S_{yz}-S_{zy} & S_{zx}-S_{xz} & S_{xy}-S_{yx} \\ S_{yz}-S_{zy} & (S_{xx}-S_{yy}-S_{zz}) & S_{xy}+S_{yx} & S_{zx}+S_{xz} \\ S_{zx}-S_{xz} & S_{xy}+S_{yx} & (-S_{xx}+S_{yy}-S_{zz}) & S_{yx}+S_{zx} \\ S_{xy}-S_{yx} & S_{zx}+S_{xz} & S_{yx}+S_{zx} & (-S_{xx}-S_{yy}+S_{zz}) \end{bmatrix},$$

where $S_{xx} = \sum_{i=1}^{n} p_{xi}q_{xi}$, $S_{xy} = \sum_{i=1}^{n} p_{xi}q_{yi}$, and so on.

The unit quaternion representing the best rotation is then found from the first eigenvector (corresponding to the largest positive eigenvalue) of $\mathbf{N}$:

$$\left[v_0, v_x, v_y, v_z\right]^\top = \underset{\mathbf{v}\in\mathbb{R}^4,\,\|\mathbf{v}\|=1}{\operatorname{argmax}}\ \mathbf{v}^\top\,\mathbf{N}\mathbf{v},$$

from which we can reconstruct the optimal rotation:

$$\mathbf{R} = \begin{bmatrix} (v_0^2+v_x^2-v_y^2-v_z^2) & 2(v_xv_y-v_0v_z) & 2(v_xv_z+v_0v_y) \\ 2(v_yv_x+v_0v_z) & (v_0^2-v_x^2+v_y^2-v_z^2) & 2(v_yv_z-v_0v_x) \\ 2(v_zv_x+v_0v_y) & 2(v_zv_y+v_0v_x) & (v_0^2-v_x^2-v_y^2+v_z^2) \end{bmatrix},$$

followed by the scaling and translation terms:

$$s = \frac{\sum_{i=1}^{n}(\mathbf{q}_i-\overline{\mathbf{q}})^\top\mathbf{R}(\mathbf{p}_i-\overline{\mathbf{p}})}{\sum_{i=1}^{n}\|\mathbf{p}_i-\overline{\mathbf{p}}\|^2} \quad \text{and} \quad \mathbf{t} = \overline{\mathbf{q}} - s\mathbf{R}\overline{\mathbf{p}},$$

where $\overline{\mathbf{p}}$ and $\overline{\mathbf{q}}$ are the centroids of the two sets of coordinates, $\overline{\mathbf{p}} = \frac{1}{n}\sum\mathbf{p}_i$ and $\overline{\mathbf{q}} = \frac{1}{n}\sum\mathbf{q}_i$. In practice it is usually possible to skip the estimation of the scaling factor and fix $s = 1$, in cases where it is known that both Ω_P and Ω_Q express coordinates in the same units (e.g. mm) and hence use the same spatial scaling.

2.1.9. Transformation of target electrode coordinates

Each electrode coordinate $\widetilde{\mathbf{p}}_i$ obtained from the neuronavigator is now transformed from the Ω_P to the Ω_Q coordinate system using

$$\widetilde{\mathbf{q}}_i = s\,\mathbf{R}\widetilde{\mathbf{p}}_i + \mathbf{t}$$

where scaling factor s, rotation matrix $\mathbf{R}$ and translation vector $\mathbf{t}$ were found in the previous step.

2.1.10. Acquire electrode coordinates on the cortical surface

Interpolate and project electrode coordinates: The final step in this method was to visualize the electrode locations relative to the cortical surface of the brain. To perform this visualization, we first rendered the 3D cortical surface from the pre-operative MRI. For this rendering, we used a combination of boundary thresholding, segmentation and surface generation tools available in the CURRY software package. An example is shown in Fig. 2(a).

In case that not all electrode coordinates have been directly acquired during surgery, it is possible to interpolate the remaining electrode positions. Such interpolation techniques take into account several factors such as grid geometry, curvature of the cortical surface and the adherence of the grid to the surface. However, such techniques (e.g., those described by Dalal et al. (Dalal et al., 2008), or those include in CURRY ver 7) introduce errors that are separate from those related to the electrode localization procedure. Because the focus of our study was to assess and validate the co-registration methodology, we acquired a set of electrode locations per subject and determined the localization errors of those electrodes prior to applying any interpolation or projection methods. Thus, our assessment of accuracy focuses on errors introduced

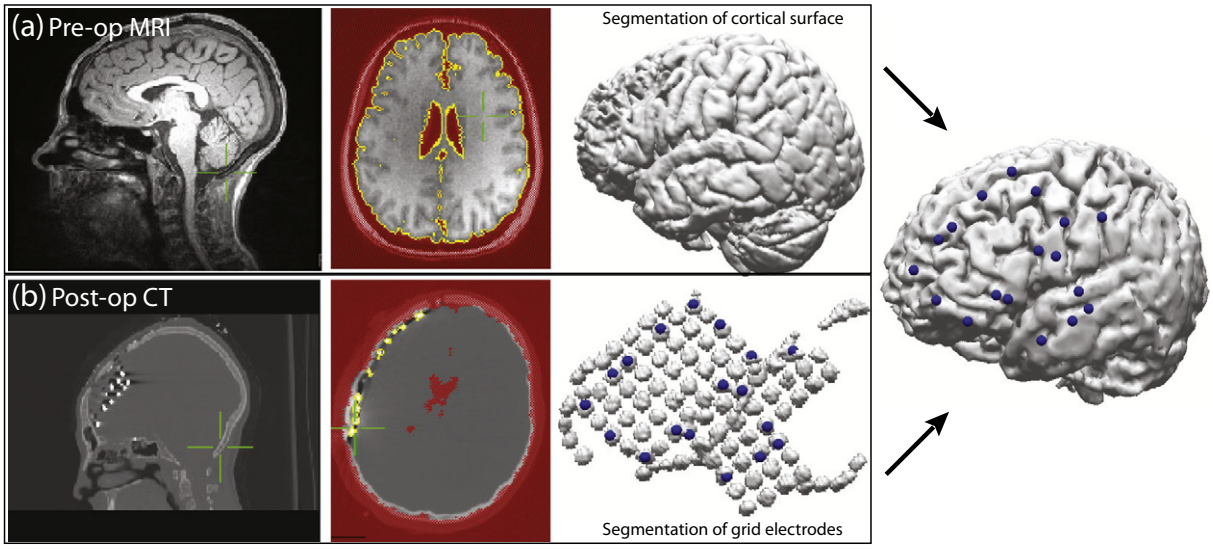

Fig. 2. The figure describes the steps taken for co-registering the pre-operative MRI and the post-operative CT to automatically extract the grid electrode locations from the clinical images. (a) The cortical surface is rendered from the high resolution structural MRI images using a combination of boundary thresholding, segmentation and surface generation tools in CURRY software. The boundaries for scalp, white matter and gray matter are also obtained here. (b) Next, the white matter boundary is overlaid on the CT images followed by segmentation and extraction of the high contrast electrodes. The electrode coordinates are then manually acquired by marking the 3D position of each visible electrode in CURRY software. The structural anatomy and the isolated electrode grid are then superimposed to obtain the electrode position relative to the cortical surface.

by the various co-registration steps and on the electrodes whose location was explicitly acquired during the surgery.

2.2. Sources of error and methods of assessment

Even using the best possible algorithms, the transformed fiducial locations will not align exactly. Errors may arise from imprecision in the physical measurement of fiducial locations in the surgical space Ω_S. They may also arise from inaccuracies in localizing fiducials in the image data, both by the neuronavigator in Ω_P and by the researcher in Ω_Q, due to image noise or the use of anatomical landmarks instead of markers. Both forms of error are referred to in the literature as *fiducial localization errors* or FLE.

In addition, systematic errors may enter the system in cases where it is impossible to avoid small physical shifts in the relative positions of the subject's head and the reference star, subsequent to neuronavigator registration.

One measure of the cumulative misalignment resulting from these sources of error is the *fiducial registration error* (FRE). We compute the vector difference between each fiducial locations $\{\mathbf{q}_i\}$ measured directly in pace and the corresponding coordinates $\{\mathbf{p}_i'\}$ measured in Ω_P and transformed into Ω_P via the estimated transform. FRE is calculated as the root mean square (RMS) of the L-2 norms of these vector differences:

$$\mathrm{FRE} = \sqrt{\frac{1}{n}\sum_{i=1}^{n} \|\mathbf{p}_i' - \mathbf{q}_i\|^2}, \quad \text{where} \quad \mathbf{p}_i' = s\,\mathbf{R}\mathbf{p}_i + \mathbf{t}.$$

However, note that FRE is a potentially *overfitted* measure because it reflects the error of an optimization procedure on its own input data. As such, it is likely to be an overoptimistic prediction of the likely error when generalizing to new target positions. One telltale sign of overfitting is that, as we shall see in Section 3.1, FRE *decreases* as the number of fiducials decreases, despite the fact that we may expect the opposite trend (to decrease errors, one must usually increase the number of data points). This explains why some previous authors found FRE to be a poor predictor of subsequent generalization errors in target registration (Fitzpatrick et al., 1998; Seginer, 2011). To compensate for this, we perform *cross-validated* (CV) tests, computing our transform on a subset of the available fiducials and computing the root-mean-square (RMS) error measure on the disjoint set of unused fiducials. The test is repeated for all possible training subsets of the same size, and the results averaged. We label the corresponding RMS error metric $\mathrm{FRE}_{\mathrm{CV}}$. Note, now, that $\mathrm{FRE}_{\mathrm{CV}}$ may be a slight underestimate of the expected generalization performance in localizing arbitrary targets on the skull, since its estimation necessarily uses a number of fiducials that has been reduced by at least 1, relative to the number we will eventually use for target localization. In our validation study, we assessed the influence of the number of fiducials by estimating FRE and $\mathrm{FRE}_{\mathrm{CV}}$ with all possible combinations of fiducial subsets having more than 3 fiducials.

$\mathrm{FRE}_{\mathrm{CV}}$ is a measure of the error one might expect when localizing points that are fixed relative to the skull. However, the localization of other targets of interest may suffer from further sources of error. There is *target localization error* (TLE) that captures the imprecision of the physical act of measuring target electrode locations in the surgical space: whereas fiducial marker mounts are designed to accept the neuronavigator probe in a particularly constrained manner, other targets of interest typically do not allow such precise localization. Furthermore, for targets on the cortex, an additional source of error is *brain shift*, i.e. shifts in the brain's position or deformations of its shape occurring between coordinate measurements and/or image acquisitions. Causes of brain shift include changes in the pressure of cerebro-spinal fluid (CSF), changes in orientation of the head (and hence the direction in which gravity acts on brain tissue) and the imposition of the weight and bulk of the electrode grid. Therefore, we are interested in the *target registration error* (TRE) computed across all m ECoG electrode targets for which we have acquired coordinates:

$$\mathrm{TRE} = \sqrt{\frac{1}{m}\sum_{i=1}^{m} \left\|\widetilde{\mathbf{p}'}_i - \widetilde{\mathbf{q}}_i\right\|^2}, \quad \text{where} \quad \widetilde{\mathbf{p}}_i' = s\,\mathbf{R}\widetilde{\mathbf{p}}_i + \mathbf{t},$$

and we must expect different results depending on whether we are interested in a cortical target, or in a target that is fixed to the skull or skin. Gumprecht et al. (1999) found that skull TRE could be as large as 4 mm ± 1.4, measuring the differences between intraoperative localization and re-localization of skull burr-holes. Ryan et al. (1996) used point-based methods in conjunction with visible landmarks (such as the center of a tumor) and estimated cortical TREs of 4.8 mm ± 3.5.

Note that TRE cannot be measured directly, because we do not have precise measurements for the ground truth $\{\tilde{\mathbf{q}}_i\}$. Rather, we can only measure the $\{\tilde{\mathbf{q}}_i\}$ using some *other* alternative localization method. The alternative method will introduce its own additional types of error. Note, therefore, that TRE is not, strictly speaking, an error measure attributable to a single method, but rather a *discrepancy between the results of two methods*, of which the relative contributions of the two methods are unknown. In the current study, we will use two such validation methods: (I) a post-operative CT method described in Section 2.4 and (II) an interoperative photograph method described in Section 2.5. The two methods' idiosyncratic sources of additional error are described in the respective sections.

We would like to highlight that in our study, the errors due to brain shift may be quite different in the two intra-operative vs. the post-operative situation. For example: post-surgery imaging may be affected by post-surgery edema; pressure on the cortex due to the combination of grid-bone-drain tubes and gravity based adjustment after CSF leakage, especially as the head is positioned differently than during surgery. On the other hand, intra-operative surgical procedures may show the most brain shift effect due to the gravitational sinking of the brain downwards with respect to the surgical plane as soon as the dura is removed and the grid is placed on the cortex. Even though there have been some demonstrations of successful estimation of brain shift errors in the MR–CT method (Hermes et al., 2010), brain shift errors have not yet been evaluated or validated for intra-operative cases. Applying the brain shift correction only on the MR–CT method clearly does not appear to be appropriate. To establish a fair comparison, we do not apply any method for brain shift correction to either the MR–CT method or our fiducial-based method, and describe our results as-is. We expect that applying brain shift correction on the MR–CT method as well the fiducial method simultaneously will reduce the net discrepancy in localization. In other words, the discrepancies that we report here are likely pessimistic estimates of their true value.

To gain insight into the effects of brain shift, particular components of TRE may also be measured. Although brain deformation is not always uniform and not exclusively in the direction of gravity (Hartkens et al., 2003; Paul et al., 2009), we hypothesized that a large component of the brain shift error would occur in a radial direction (i.e., normal to the cortical surface at the position of the electrode). This is because the CSF pressure and gravity are most likely to act along this axis during the surgery with respect to the plane of the surgery. Therefore, in our analyses, we compute the magnitude of the radial component of TRE as well as the remaining tangential component (i.e., the RMS magnitude of the TRE vectors that had their radial component removed).

Also, for validation method II, the final TRE is computed from a two-dimensional projection. Therefore, in our comparison of the two validation methods, we use the same two-dimensional projection for both validation methods before computing TRE.

Finally, an approach for assessing the magnitude of errors due to brain shift and grid shift, while avoiding the overconfidence of *FRE* or the pessimism of FRE_{CV}, is to acquire additional target locations on the skull and their *TRE* with the *TRE* of grid targets. If bone screws are inserted to secure the bone flap when closing the craniotomy, these provide ideal fixed targets for such a test. In our study, we were able to acquire the locations of bone screws for one of our subjects. The screws were of cross-head type, with a small cross-shaped groove that provided an accurate reference point for placement of the navigation probe. As these screws are fastened to the bone, they cannot be displaced. Also, the deformation of the skull bone should be only minuscule. Thus, we hypothesized that a cortical deformation, where the grid tends to sink unpredictably, would affect the transformed grid coordinates more than the transformed screw coordinates. The difference between the grid and screw coordinate localization errors could then be used for compensating the translational error in the direction of gravity. We tested this hypothesis by acquiring the 3D coordinates of 6 bone screws during the grid implantation surgery and in the post-operative CT images (see Fig. 5(a)).

2.3. Validation methods

2.3.1. Human subjects

The data used for this study included six patients with drug-resistant epilepsy who were candidates for resective surgery for epilepsy. The subjects were recruited, with informed consent, at the Epilepsy Monitoring Unit at Albany Medical Center (AMC) in Albany, New York. As part of their clinical evaluation and surgical planning, subdural electrodes were temporarily implanted for a few days to allow the clinicians to localize the seizure focus and to delineate eloquent cortex. Electrodes were of 4 mm diameter (2.3 mm exposed surface) embedded in a transparent silastic material with an inter-electrode distance of 10 mm. All data were collected with approval by the Institutional Review Board of AMC. A brief clinical profile of the subjects is given in Table 1.

2.3.2. Acquisition of validation data

Pre-operative MRI scans were available for all patients, but were taken before the day of the operation and did not include fiducial markers.

Our method will provide optimal benefit if no post-operative imaging is available. However, to be able to validate our method, we included only patients in our study who underwent a two-stage procedure with a grid-implantation and who had both pre- and post-operative CT imaging. The pre-operative CT included fiducial markers for the purpose of neuronavigator registration, as described in the procedure above. Post-operative CT imaging was performed within 24 h of grid implantation to verify the grid location after closing and to check for edema. Like the pre-operative CT, it was taken skin-to-skin with 1 mm slice width and no angle.

As part of a second validation method, two photographs were taken during the surgery. The first photo captured the cortical surface where the grid was about to be placed, with a clear view of the vasculature, sulcal patterns, and craniotomy edges. The second photo captured the same area but with the grid placed on the cortical surface, such that the underlying cortical and vasculature patterns were visible through the grid. Where the constraints of the surgery allowed it, we used the OPMI Pentero surgical microscope (Carl Zeiss Meditec, Inc., USA) to ensure that the two photographs were of high resolution and taken from the same position and angle. In other cases, we used a handheld camera and replicated the angle as closely as possible.

Table 1
Clinical profiles of the subjects that participated in the study.

Subject	Age	Sex	Grid/strip location	Num. of electrodes
1	60	M	Left parieto-occipital	35
			Left temporo-occipital	6
			Left occipital lateral, mesial	4, 4, 4
			Left occipital frontal	6
2	26	F	Left temporal	78
			Left fronto-temporal	36
			Left inferior temporal	4, 4
			Left temporo-occipital	6
3	12	M	Left fronto-temporal	63, 8
			Left frontal inter-hemispheric	12, 3, 3, 4
4	16	F	Right frontal	49
			Right temporal strip	6, 4
			Inter-hemispheric frontal	8
			Occipital strip	4
5	27	M	Right frontal	44
			Right temporal, mesial	35, 6
			Occipital strip	4
			Bone screws	6
6	*	M	Left frontal	61

* Missing.

2.4. Validation I (post-operative CT method)

Localization with a pre-operative MRI and a post-operative CT has been demonstrated in several studies (Dykstra et al., 2012; Grzeszczuk et al., 1992; Hermes et al., 2010; Sebastiano et al., 2006; Tao et al., 2009; Winkler et al., 2000). In our implementation, the post-operative CT showing the implanted grid was co-registered to the pre-operative MRI using the same procedure described in Section 2.1.7.

The 3D structure of the grid was then rendered following thresholding of the CT by importing the skin and bone boundaries detected in the co-registered MRI followed by segmentation of the CT volume with thresholding to isolate only the grid. Example results of this rendering process are shown in Fig. 2(b).

The 3D coordinates of the target electrodes are then acquired manually and saved for validation.

In addition to the brain-shift error discussed in Section 2.2, this method can be expected to introduce errors from imperfect co-registration of the post-operative CT and MRI, from imprecise 3-D rendering of electrodes (particularly if the grid is dense, because the electrode volumes tend to merge), and from imprecise manual acquisition of the electrode coordinates. Furthermore, in rare cases the grid may shift in transit between the OR and the CT due to gravity or due to tension in its cables. Finally, post-surgical edema may cause an additional component of brain shift, above and beyond the brain shift that occurs between the pre-operative MRI and the OR.

2.5. Validation II (intra-operative photograph method)

Localization by pre-operative MRI and intra-operative photographs has also been investigated by a number of authors, such as Dalal et al. (2008), Wellmer et al. (2002), and Hermes et al. (2010). As described in these methods, first we highlighted the vasculature and craniotomy boundary on the intra-operative digital photograph that displayed the exposed cortical surface before grid placement, see Fig. 3 panels (a) and (c). Next, we highlighted the grid, visible vasculature and craniotomy boundary on the second intra-operative photograph, obtained after grid placement, as shown in panels (b) and (d). Then, we manually merged the 2 photographs with the highlighted structures resulting in a clearer view of the grid and the underlying patterns, as shown in panel (e). If the photographs were not taken from the same fixed camera position and angle, we manipulated the photographs in a non-rigid manner. The editing was performed in Adobe Photoshop (Adobe Systems, Inc., USA). Then, we rendered the 3D cortical model from the pre-operative MRI, as described in Section 2.1.10. Next, we highlighted the sulcal patterns (generally known to coincide with the main vasculature patterns) at the known craniotomy location on this 3D anatomical structure, shown in panel (f). We projected the electrodes localized by the previous two methods on to this structure as well. Finally, we aligned the view of the 3D cortical surface with the superimposed image of the grid and cortical structures, using prominent anatomical landmarks such as the Sylvian fissure or other discernible sulcal and vasculature patterns (h). We quantified the discrepancy between the localized electrode coordinates using the two-dimensional Euclidean norm.

In addition to the brain-shift error discussed in Section 2.2, this method can be expected to introduce errors from imperfect volume reconstruction of the MRI, from manual error in matching the 2D image to the MRI rendering, and from manual error in matching the 2D "before" image to the 2D "after" image (particularly when the electrode grid is dense, or when it is placed in a region in which vascular landmarks can not readily be identified).

3. Results

The subdural ECoG grid electrodes were localized for the 6 subjects using our procedure, and validated with the commonly used techniques of MRI–CT co-registration as well as intra-operative photograph method. The upper panels of Fig. 4 show the 3D rendered cortex models of the 6 subjects, together with estimated target locations from our point-based procedure (green) and those of validation method I, the MR–CT method of Section 2.4 (red). Qualitatively, the two sets of coordinates can be seen to be in close agreement. Quantitative results are plotted in the bottom two panels of the figure.

3.1. Validation results: scalp and skull targets

We estimate the inherent error of the point-based registration method using the FRE and FRE_{CV} error metrics as described in section 2.2. The bars in panel (a) on the lower right of Fig. 4 show FRE and FRE_{CV} as a function of number of fiducials used for transform estimation. Each blue bar shows an average FRE, computed for each possible fiducial subset of a given size, then averaged across subsets, then averaged across subjects. We can see that FRE increases as a function of the number of fiducials, as it becomes harder for the optimization procedure to learn the set of fiducials exactly. This is to be expected when reporting an optimization algorithm's loss metric computed on its own training set, and is not indicative of generalization performance. The red bars show FRE_{CV}: each red bar was computed by taking all possible fiducial subsets of a given size, and then, for each subset, evaluating FRE_{CV} by training on that subset and testing on the remaining available fiducials. The FRE_{CV} values were then averaged per-subject across all subsets, and then averaged across subjects. In contrast to FRE, FRE_{CV} decreases as the number of fiducials increases. These results demonstrate that the application of the transform improves on unseen targets as an increasing number of fiducials are used in estimation of transformation parameters. FRE and FRE_{CV} appear to converge at slightly more than 2 mm. Using all but one fiducial for each subject (two of our subjects had as many as 10 fiducials), the leave-one-out FRE_{CV} was 2.39 mm on average across subjects. The qualitative trends, as well as the numerical value of this estimate of the intrinsic imprecision of point-based registration, are very similar to the results reported by Kwartowitz et al. (2006).

3.2. Validation results: cortical targets

The TRE, reflecting the discrepancy between our method and the MR–CT grid coordinate localization results, is much larger than the FRE, as shown in panel (b) at the bottom right of Fig. 4. Mean FRE_{CV} and TRE across subjects were computed using as many fiducials as possible for each subject, and these are shown as total error, and then broken down into radial and non-radial components. We also note that, on average across the subjects, TRE changed only very slightly (from 8.4 mm to 8.25 mm) as the number of fiducials increased from 3 to 7 (results not shown). Taken together with the large difference between TRE and FRE_{CV} values, this suggests that the majority of our TRE does not come from fiducial localization error or from inaccuracies of registering fixed points in general, but rather from problems in localizing targets on the cortical grid—with the associated problems of target localization error and brain shift. Furthermore, note that TRE is not dominated by the radial component (total TRE has a mean of 8.24 mm and a median of 7.10 mm across subjects, whereas radial TRE has mean 4.76 mm and median 3.49 mm). This suggests that the problem does not purely come from intraoperative brain shift in the direction of gravity. It may be due to reference-frame shift during the operation, due to errors introduced in the MR–CT method used for validation, or due to errors in the proposed fiducial method.

The use of bone screws provided a further opportunity to diagnose sources of error in subject 5. With this subject, we achieved a leave-one-out FRE_{CV} of 2.67 mm. We also estimated the radial components of localization error for electrodes placed on the cortex (affected by brain shift) vs. screws on the bone (not affected by brain shift). The bone screws showed a smaller radial localization error of 1.26 mm as compared to the grid electrodes' radial localization error of 4.48 mm,

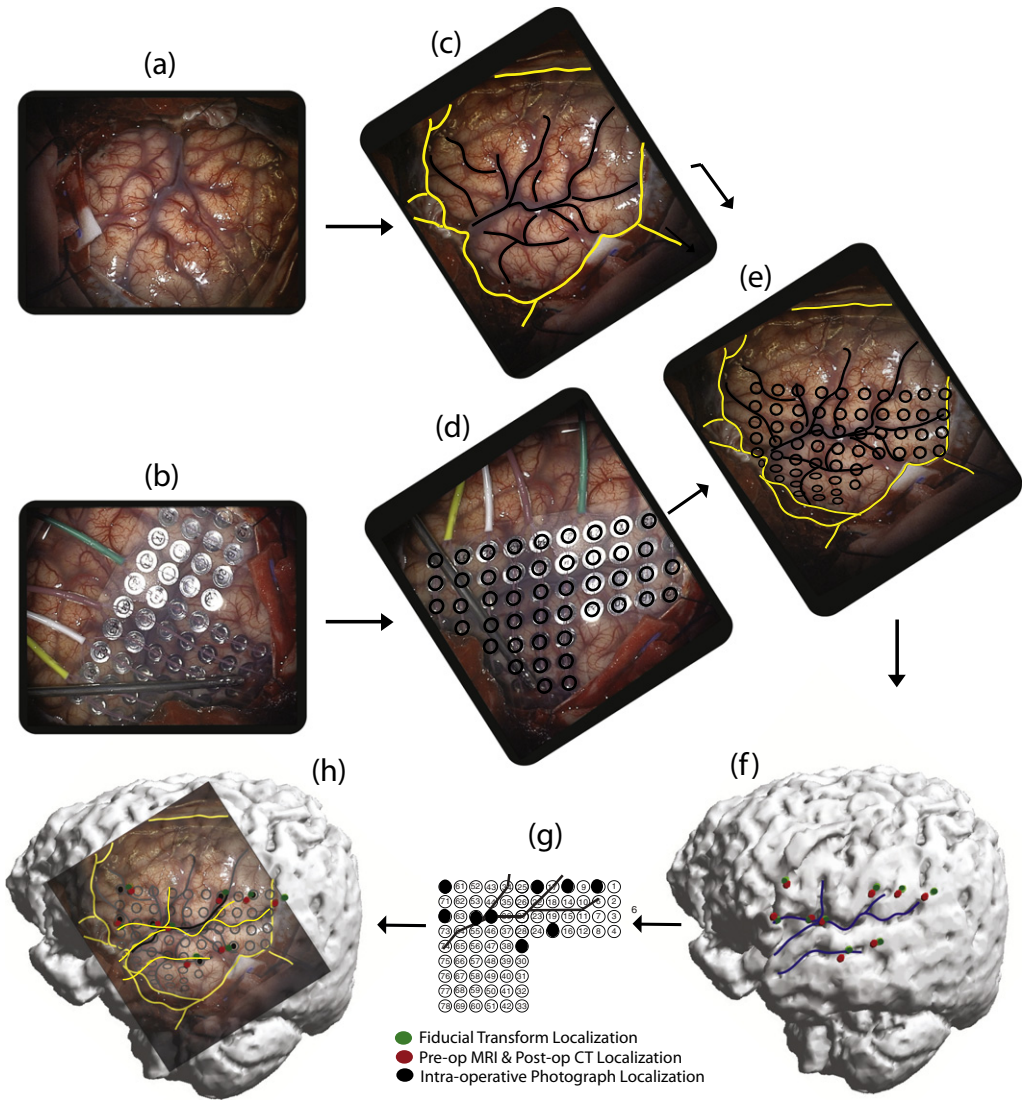

Fig. 3. Localization of grid electrodes using intra-operative photographs. (a) Photograph of the exposed cortical surface taken before the grid is placed. (b) Photograph of the same surface after the grid has been placed. (c, d, e) Cortical surface and grid with highlighted vasculature and grid electrodes, nonlinearly rotated followed by their superimposition. (f) Prominent sulcal patterns marked on the 3D cortical surface (cortex was reconstructed from the pre-operative MRI). (g) Grid electrodes whose coordinates were acquired intra-operatively. (h) Intra-operative photographs of the grid (matched to the cortical surface) superimposed on the 3D cortical surface, allowing the measurement of electrode localization discrepancy using the three localization techniques.

in the same subject and during the same procedures. In comparison to the MR–CT validation method, the TRE for 6 bone screws (5.90 mm) was less than the TRE for 10 cortical targets (9.04 mm), but it is still more than double the error we experience when localizing fiducials based on other fiducials. Both screw and electrode targets are susceptible to errors in the MR–CT method itself, and to shifts in the surgical reference frame following neuronavigator registration, whereas only the electrodes are susceptible to brain shift and grid shift. Thus, the use of bone screws for estimating localization errors provides an estimate of the relative contributions of the different error sources. The screw positions are shown in Fig. 5. Note that the small bone screw errors appear to be in a consistent posterior–inferior direction, whereas the grid target errors appear to be in a consistent anterior–inferior direction. The most likely interpretation of this is that errors common to both target types (either from reference-frame shift or from errors endemic to the MR–CT validation method) caused the systematic posterior–inferior error for this subject; a combination brain shift and grid shift may then have added an anterior-directed component to this error vector.

In Fig. 6, we plot our estimates of the discrepancy in localization between our point-based method and the intra-operative photograph method (validation method II), as well as the MR–CT method (validation method I). Errors for the photographic method must be computed on a two-dimensional projection. Because their magnitudes are different, they cannot readily be compared with errors estimated from 3D models in Fig. 4. Therefore, to make a fair comparison with other methods, we obtained 2-D projected coordinates for our point-based method as well as for the MR–CT validation method, and computed TRE values between all pairs of methods in this coordinate system. To obtain the 2D coordinates from the electrodes projected on a 3D cortex, we first project both the fiducial-localized electrodes and the MR–CT localized electrodes onto the 3D cortex. We then orient the 3D cortex such that it matches the intra-operative photograph section in scale and orientation. We further align the cortex with the photograph using anatomical/structural landmarks, as depicted in Fig. 3. Once they are aligned, we obtain the x and y coordinate positions of the electrodes on the photograph and the electrode positions of both – the MR–CT as well as the fiducial based electrodes – from the aligned 3D cortex. This allows us to compare the discrepancy among the three groups as shown in Fig. 6.

On this scale, agreement between our method and the photo method was 2.7 mm ± 0.7 (mean ± standard deviation across

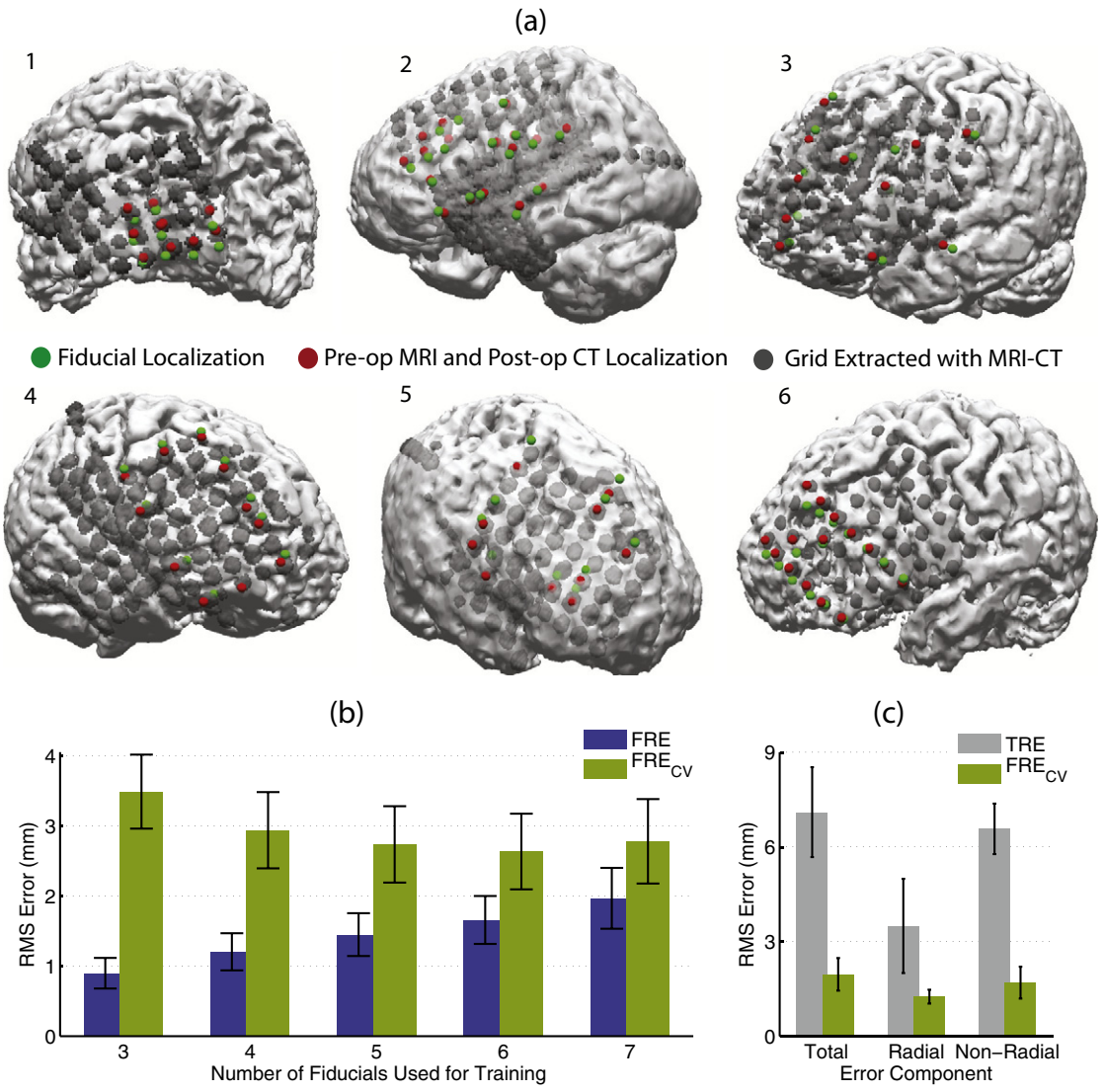

Fig. 4. Upper panel: 3D cortical surfaces of the subjects reconstructed by their individual pre-operative MRI images. Red spheres: the grid electrode positions that were probed during the surgery. Green spheres: the electrode positions localized with our fiducial-based technique. Gray spheres: the grid extracted with the pre-operative MRI and post-operative CT co-registration procedure. Lower panel: 3D errors. (a) The RMS of fiducial registration error (FRE, blue) and the cross-validated fiducial-as-target error (FRE_{CV}, green), averaged across all subjects, as a function of the number of fiducials used. Panel (b) shows the comparison between FRE_{CV} in green (estimated on fiducials using a leave-one-out procedure for each subject) and the discrepancies (TRE) between our point-based method and the MR–CT validation method, in gray. Mean ± standard error across subjects is shown for total error, and separately for just the radial and non-radial components of the error.

subjects). Agreement between our method and the MR–CT method was 3.73 mm ± 2.4, and agreement between the two validation methods (photo and MR–CT) was 3.1 mm ± 1.9. The figure shows the three types of discrepancy for each subject. It should be noted that, for the two subjects in which our point-based method has the largest TRE relative to MR–CT coordinates, the two validation methods also diverge to a large extent from each other. This may be a further indication that the MR–CT validation method is itself introducing a large proportion of the error into our assessment.

3.3. Application: intra-operative localization of micro-grid

Finally, we demonstrate an application of this method in a single-stage surgery where no post-operative imaging was available. The subject, subject number 6 from the above dataset, had undergone a routine two-stage ECoG monitoring with a 64-channel grid (see panel 6 in Fig. 4). However, during the second surgery, additional functional mapping was performed using a high-resolution micro-grid. The electrodes of the smaller grid were localized and validated as described in the previous sections.

Fig. 7(a) shows electrode positions on the 64-channel macro-grid that had been implanted at the beginning of the monitoring period (blue spheres). The macro-grid was removed, the micro-grid was placed and its electrodes were acquired in the Ω_P and Ω_Q. Target positions on the micro-grid, acquired as described in Section 2.1.6, are shown in red.

Fig. 7(b) shows the results of passive functional mapping using auditorily-cued verb generation and the SIGFRIED method (Brunner et al., 2009; Schalk et al., 2008). The blue circles represent results from a mapping session performed during the monitoring period. Significance of task-related activation in the gamma band (70–170 Hz), reflected by the size and lightness of the circle at each electrode position. These maps indicate cortical areas under three electrodes in Broca's Area (Brodmann Area 44–45) that are involved in verb generation. The red circles show the results from the same task, repeated intraoperatively using the micro-grid (circle sizes are not on the same scale for the two grids). It can be seen that the electrodes in the micro-grid that

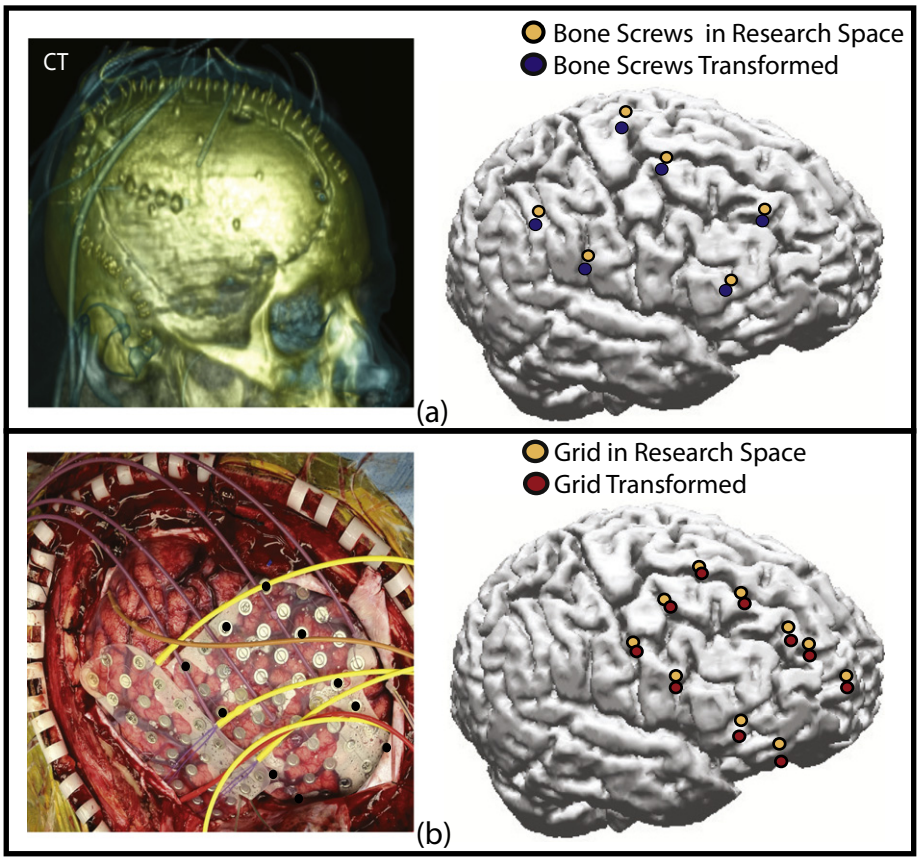

Fig. 5. (a) Bone screw points as shown on the CT, as acquired by the MRI–CT method (orange) and after application of the fiducial-based transform (blue); (b) grid electrodes as shown on the intra-operative photograph, as acquired by the MRI–CT method (orange) and after application of the fiducial based transform (red).

show significant activations during verb generation are largely in the area where the electrodes from the macro-grid show task related activations for the same task. Moreover, the micro-grid further delineates eloquent areas within the inter-electrode cortical areas where the macro-grid fails to capture any information. This concordance of the functional mapping, with increased resolution, illustrates the way in which our localization method can provide increased detail in registering function and anatomy in cases where resolution would otherwise be limited by the large inter-electrode spacing of the grid (1 cm). Higher-resolution coverage of a large spatial area with high-density grids would be ideal for clinical and research purposes to map cortical functions more precisely. In summary, our fiducial-based grid localization method allowed us to localize the electrodes of this micro-grid, which was only available intraoperatively and was too dense to make underlying anatomical landmarks visible.

4. Discussion

ECoG grids are routinely placed subdurally on the cortex in people with epilepsy to delineate cortical areas involved in seizures or function. These grids provide exceptional opportunities for neuroscientific research, because they detect signals from the brain at high spatial

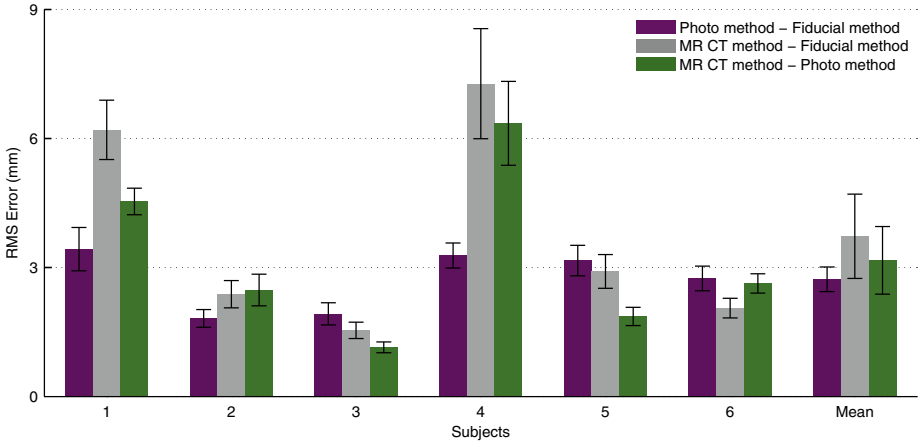

Fig. 6. Validation results: 2D projected localization discrepancies between our point-based grid electrode localization and the photograph-based localization of method II (purple), between our method and the MRI–CT based localization of validation method I, (gray), and between the two validation methods (green). The average errors are 2.7 mm, 3.72 mm and 3.16 mm, respectively.

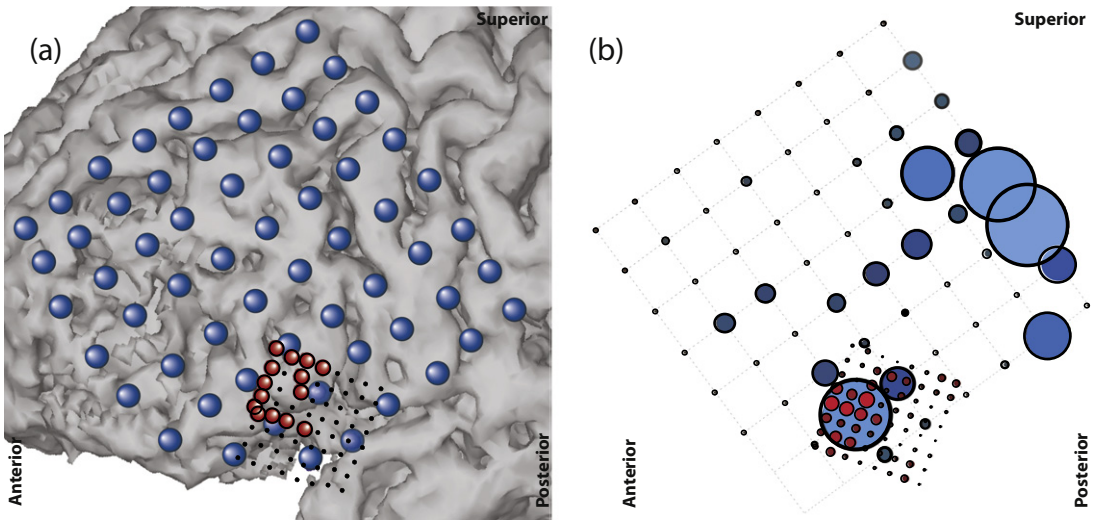

Fig. 7. (a) Stage 1: Functional mapping for verb generation performed using the SIGFRIED method using recordings from a macro-grid (inter-electrode distance of 1 cm) placed subdurally for monitoring epileptic seizures. (b) Stage 2: Functional mapping for verb generation performed with a micro-grid (inter-electrode distance of 3 mm) placed subdurally during an awake craniotomy. The red circles on SIGFRIED maps represent task-related activations in the gamma band (70–170 Hz). The size and color of each circle indicate the magnitude of the effect.

and temporal resolution. Relating these signals to the underlying anatomy requires co-registering the location of the electrodes to the location of the anatomy. Existing methods that support this co-registration use pre-operative magnetic resonance imaging (MRI), which captures the cortical anatomy, and post-operative computerized tomography (CT), or X-Rays that capture the electrode locations. However, when ECoG grids are not implanted but only temporarily placed during a surgery, there is no post-operative imaging that includes the grid. Other existing methods make use of intra-operative photographs, but they require a great deal of manual adjustment (with results varying widely according to the researcher's skill and time invested). They also require that the electrodes be visually related to the underlying anatomy, which can be difficult or even impossible (e.g. with high-density grids). These limitations of existing localization techniques limit the potential value of the interpretation of ECoG signals collected during single-stage surgeries.

The existing method that co-registers a pre-operative MRI with a post-operative CT is affected by the errors in MRI and CT imaging, volume reconstruction, interpolation artifacts, segmentation thresholds, deformation and grid shift. In surgeries that involve a craniotomy, it is also not uncommon for brain deformation to take place by the time the dura is closed and the patient is taken for post-operative imaging (Hartkens et al., 2003). Unpredictable, non-uniform shifts, as high as 20 mm have been observed (Hartkens et al., 2003). A number of reasons may cause such deformations, such as CSF leakage, post-operative trauma, gravity, cortex receding from the bone, and pressure exerted by the grid (Etame et al., 2011). Consequently, the cortical boundary imaged with a pre-operative MRI may not accurately match that obtained using a post-operative CT. This increases the discrepancy between the electrodes localized intra-operatively with the fiducial-based method and one that used a pre-operative MRI and post-operative CT. Grid localization errors of 6 mm or more are not uncommon (Hastreiter et al., 2004).

Such a discrepancy can be measured to a certain extent by either disregarding the component of discrepancy that is in the direction of the gravity or by using fixed fiducials where the fiducials themselves, or the surface on which they are placed, cannot vary. We explored both these variations in order to ascertain the minimal intrinsic errors of the fiducial based method. First, we assessed the radial error by estimating the component of TRE that was normal to the surface of the grid (and the cortical surface), as the grid and cortical surface is perpendicular to the direction of gravity during surgery. We then assessed the localization error for the fixed fiducials (i.e., the screws) by acquiring the 3D coordinates of bone screws that the surgeon secured to the bone for replacing the bone flap. As expected, the screws showed a smaller radial error than the cortical grid targets. All point coordinates are measured with reference to the center of the brain, i.e., the junction of the AC–PC line and the midline.

In three dimensions, the intrinsic error of the method for localizing fixed (scalp- or skull-mounted) targets was estimated to around 2.4 mm, averaged across our 6 subjects, and our method agreed with a method based on post-operative CT method to within 8.24 mm on average. In a two-dimensional projection, our method agreed with manual registration of intra-operative digital photographs to within 2.72 mm on average. As discussed, these discrepancies include the endogenous errors of each of the methods.

Furthermore, some electrodes can also get pushed under the dura and become inaccessible to direct navigation during the surgery. To extract the coordinates of these electrodes, one can use the grid geometry and the curvature of the cortical surface to interpolate the inaccessible electrode positions (Dalal et al., 2008). We only validated the localization accuracy of electrodes that can be probed during the surgery, i.e., electrodes that are within the trepanation. In case it is necessary to recover the entire grid (i.e., not only electrodes that were sampled, but also others), it is necessary to interpolate those additional electrode locations. Because the accuracy of this interpolation step depends strongly on a number of different factors (such as number and nature of sampled electrodes and degree of brain curvature), we recommend to sample as many electrodes as possible, in particular alternate grid corner, or complete squares.

It should be noted that our fiducial-based method does not specifically rely on commercial software (such as CURRY) for co-registration and extracting coordinates. Co-registration and coordinate extraction functionality is also readily available in open-source software such as SPM (http://www.fil.ion.ucl.ac.uk/spm/).

In summary, we developed and validated a point-based method using fiducial markers to co-register ECoG electrodes to the underlying cortical anatomy when post-operative imaging is not available, such as during single-stage intra-operative studies. Our procedure should prove useful for research using ECoG data collected during single-stage intra-operative scenarios. It will provide maximal benefit in situations in which post-operative imaging is not available or is not useful (e.g. intra-operative photographs that do not readily show the relationship between anatomical landmarks and electrode locations). This method

can also be integrated with real-time mapping tools that can help to delineate the eloquent cortex at a much higher spatial resolution during the surgery.

Acknowledgments

This work was supported in part by grants from the US Army Research Office [W911NF-08-1-0216 and W911NF-07-1-0415] and the NIH [EB006356 and EB000856]. The authors would like to thank the staff of AMC surgical unit, especially Dr. Ravi Gandhi, Dr. Farhad Bahrassa, Dr. Walter and Dr. Amilyn Taplin, for their cooperation and technical support. We would also like to thank Phil Schrom from PMT and Dr. Guenter Edlinger from g.tec for their valuable support during the development of the micro-grid.

References

Brunner, Peter, Ritaccio, Anthony L., Lynch, Timothy M., Emrich, Joseph F., Adam, J., Williams, Justin C., Aarnoutse, Erik J., Ramsey, Nick F., Leuthardt, Eric C., 2009. A practical procedure for real-time functional mapping of eloquent cortex using electrocorticographic signals in humans. Epilepsy Behav. 15 (3), 278–286.

Chang, E.F., Rieger, J.W., Johnson, K., Berger, M.S., Barbaro, N.M., Knight, R.T., 2010. Categorical speech representation in human superior temporal gyrus. Nat. Neurosci. 13 (11), 1428–1433.

Crone, N.E., Boatman, D., Gordon, B., Hao, L., 2001. Induced electrocorticographic gamma activity during auditory perception. Brazier Award-winning article, 2001. Clin. Neurophysiol. 112 (4), 565–582.

Crone, N.E., Sinai, A., Korzeniewska, A., 2006. High-frequency Gamma Oscillations and Human Brain Mapping With Electrocorticography. Progress in Brain Research. vol. 159, pp. 275–295.

Dalal, S., Edwards, E., Kirsch, H.E., Barbaro, N.M., Knight, R.T., Nagarajan, S.S., 2008. Localization of neurosurgically implanted electrodes via photograph–MRI–radiograph coregistration. J. Neurosci. Methods 174 (1), 106–115.

Dykstra, A.R., Chan, A.M., Quinn, B.T., Zepeda, R., Keller, C.J., Cormier, J., Madsen, J.R., Eskandar, E.N., Cash, S.S., 2012. Individualized localization and cortical surface-based registration of intracranial electrodes. NeuroImage 59 (4), 3563–3570.

Eggert, D.W., Lorusso, A., Fisher, R.B., 1997. Estimating 3-D rigid body transformations: a comparison of four major algorithms. Mach. Vis. Appl. 9 (5–6), 272–290.

Etame, A.B., Fox, W.C., Sagher, O., 2011. Osmotic diuresis paradoxically worsens brain shift after subdural grid placement. Acta Neurochir. 153 (3), 633–637.

Fitzpatrick, J. Michael, West, J.B., Maurer Jr., C.R., 1998. Predicting error in rigid-body point-based registration. IEEE Trans. Med. Imaging 17 (5), 694–702.

Flinker, A., Chang, E.F., Barbaro, N.M., Berger, M.S., Knight, R.T., 2011. Sub-centimeter language organization in the human temporal lobe. Brain Lang. 117 (3), 103–109 Jun.

Grzeszczuk, R., Tan, K.K., Levin, D.N., Pelizzari, C.A., Hu, X., Chen, G.T.Y., Beck, R.N., Chen, C.-T., Cooper, M., Milton, J., Spire, J.-P., Towle, V.L., Dohrmann, G.J., Erickson, R.K., 1992. Retrospective fusion of radiographic and MR data for localization of subdural electrodes. J. Comput. Assist. Tomogr. 16 (5), 764–773.

Gumprecht, H.K., Widenka, D.C., Lumenta, C.B., 1999. BrainLab VectorVision Neuronavigation System: technology and clinical experiences in 131 cases. Neurosurgery 44 (1), 97–104.

Gunduz, Aysegul, Brunner, Peter, Daitch, Amy, Leuthardt, Eric C., Ritaccio, Anthony L., Pesaran, Bijan, Schalk, Gerwin, 2012. Decoding covert spatial attention using electrocorticographic (ECoG) signals in humans. NeuroImage 60 (4), 2285–2293.

Hartkens, T., Hill, D.L.G., Castellano-Smith, A.D., Hawkes, D.J., Maurer, C.R., Martin, A.J., Hall, W.A., Liu, H., Truwit, C.L., 2003. Measurement and analysis of brain deformation during neurosurgery. IEEE Trans. Med. Imaging 22 (1), 82–92.

Hastreiter, P., Rezk-Salama, C., Soza, G., Bauer, M., Greiner, G., Fahlbusch, R., Ganslandt, O., Nimsky, C., 2004. Strategies for brain shift evaluation. Med. Image Anal. 8 (4), 447–464.

Hermes, D., Miller, K.J., Noordmans, H.J., Vansteensel, M.J., Ramsey, N.F., 2010. Automated electrocorticographic electrode localization on individually rendered brain surfaces. J. Neurosci. Methods 185 (2), 293–298.

Hill, N.J., Gupta, D., Brunner, P., Gunduz, A., Adamo, M.A., Ritaccio, A., Schalk, G., 2012. Recording human electrocorticographic (ECoG) signals for neuroscientific research and real-time functional cortical mapping. J. Vis. Exp. (64), 1–5.

Horn, B.K.P., 1987. Closed-form solution of absolute orientation using unit quaternions. J. Opt. Soc. Am. 4, 629 (April).

Kellis, S.S., House, P.A., Thomson, K., Brown, R., Greger, B., 2010. Human neocortical electrical activity recorded on nonpenetrating microwire arrays: applicability for neuroprostheses. Neurosurg. Focus 27 (1), 1–18.

Kovalev, D., Spreer, J., Honegger, J., Zentner, J., Schulze-Bonhage, A., Huppertz, H.-J., 2005. Rapid and fully automated visualization of subdural electrodes in the presurgical evaluation of epilepsy patients. Am. J. Neuroradiol. 26 (5), 1078–1083.

Kubanek, J., Miller, K.J., Ojemann, J.G., Wolpaw, J.R., Schalk, G., 2009. Decoding flexion of individual fingers using electrocorticographic signals in humans. J. Neural Eng. 6 (6), 066001.

Kuehn, B., Mularski, S., Schoenherr, S., Hammersen, S., Stendel, R., Kombos, T., Suess, S., Suess, O., 2008. Sensor-based neuronavigation: evaluation of a large continuous patient population. Clin. Neurol. Neurosurg. 110 (10), 1012–1019.

Kwartowitz, D.M., Herrell, S.D., Galloway, R.L., 2006. Toward image-guided robotic surgery: determining intrinsic accuracy of the da Vinci robot. Int. J. Comput. Assist. Radiol. Surg. 1 (3), 157–165.

LaViolette, P.S., Rand, S.D., Ellingson, B.M., Raghavan, M., Lew, S.M., Schmainda, K.M., Mueller, W., 2011. 3D visualization of subdural electrode shift as measured at craniotomy reopening. Epilepsy Res. 94 (1–2), 102–109.

Miller, K.J., Leuthardt, E.C., Schalk, G., Rao, R.P.N., Anderson, N.R., Moran, D.W., Miller, J.W., Ojemann, J.G., 2007a. Spectral changes in cortical surface potentials during motor movement. J. Neurosci. 27 (9), 2424–2432.

Miller, K.J., Makeig, S., Hebb, A.O., Rao, R.P.N., DenNijs, M., Ojemann, J.G., 2007b. Cortical electrode localization from X-rays and simple mapping for electrocorticographic research: the "location on cortex" (LOC) package for MATLAB. J. Neurosci. Methods 162 (1–2), 303–308.

Mutic, S., Dempsey, J.F., Bosch, W.R., Low, D.A., Drzymala, R.E., Chao, K.S., Goddu, S.M., Cutler, P.D., Purdy, J.A., 2001. Multimodality image registration quality assurance for conformal three-dimensional treatment planning. Int. J. Radiat. Oncol. Biol. Phys. 51 (1), 255–260.

Paul, P., Morandi, X., Jannin, P., 2009. A surface registration method for quantification of intraoperative brain deformations in image-guided neurosurgery. IEEE Trans. Inf. Technol. Biomed. 13 (6), 976–983.

Pei, Xiaomei, Leuthardt, Eric C., Gaona, Charles M., Brunner, Peter, Wolpaw, Jonathan R., Schalk, Gerwin, 2011. Spatiotemporal dynamics of electrocorticographic high gamma activity during overt and covert word repetition. Neuroimage 54 (4), 2960–2972.

Ryan, M.J., Erickson, R.K., Levin, D.N., Pelizzari, C.A., Macdonald, R.L., Dohrmann, G.J., 1996. Frameless stereotaxy with real-time tracking of patient head movement and retrospective patient–image registration. J. Neurosurg. 85 (2), 287–292.

Schalk, G., Kubanek, J., Miller, K.J., Anderson, N.R., Leuthardt, E.C., Ojemann, J.G., Limbrick, D., Moran, D., Gerhardt, L.A., Wolpaw, J.R., 2007. Decoding two-dimensional movement trajectories using electrocorticographic signals in humans. J. Neural Eng. 4 (3), 264.

Schalk, G., Leuthardt, E.C., Brunner, P., Ojemann, J.G., Lester, A., Wolpaw, J.R., 2008. Real-time detection of event-related brain activity. Neuroimage 43 (2), 245–249.

Schulze-Bonhage, A.H.-J., Huppertz, H.J., Comeau, R.M., Honegger, J.B., Spreer, J.M., Zentner, J.K., 2002. Visualization of subdural strip and grid electrodes using curvilinear reformatting of 3D MR imaging data sets. AJNR Am. J. Neuroradiol. 23 (3), 400–403.

Sebastiano, F., Di Gennaro, G., Esposito, V., Picardi, A., Morace, R., Sparano, A., Mascia, A., Colonnese, C., Cantore, G., Quarato, P.P., 2006. A rapid and reliable procedure to localize subdural electrodes in presurgical evaluation of patients with drug-resistant focal epilepsy. Clin. Neurophysiol. 117 (2), 341–347.

Seginer, A., 2011. Rigid-body point-based registration: the distribution of the target registration error when the fiducial registration errors are given. Med. Image Anal. 15 (4), 397–413.

Silberbusch, M.A., Rothman, M.I., Bergey, G.K., Zoarski, G.H., Zagardo, M.T., 1998. Subdural grid implantation for intracranial EEG recording: CT and MR appearance. Am. J. Neuroradiol. 19 (6), 1089–1093.

Sinai, A., Bowers, C.W., Crainiceanu, C.M., Boatman, D., Gordon, B., Lesser, R.P., Lenz, F.A., Crone, N.E., 2005. Electrocorticographic high gamma activity versus electrical cortical stimulation mapping of naming. Brain 128, 1556–1570.

Sinai, A., Crone, N.E., Wied, H.M., Franaszczuk, P.J., Miglioretti, D., Boatman-Reich, D., 2009. Intracranial mapping of auditory perception: event-related responses and electrocortical stimulation. Clin. Neurophysiol. 120 (1), 140–149.

Tao, J.X., Hawes-Ebersole, S., Baldwin, M., Shah, S., Erickson, R.K., Ebersole, J.S., 2009. The accuracy and reliability of 3D CT/MRI co-registration in planning epilepsy surgery. Clin. Neurophysiol. 120 (4), 748–753.

Ulin, K., Urie, M.M., Cherlow, J.M., 2010. Results of a multi-institutional benchmark test for cranial CT/MR image registration. Int. J. Radiat. Oncol. Biol. Phys. 77 (5), 1584–1589.

Van Gompel, J.J., Stead, S.M., Giannini, C., Meyer, F.B., Marsh, W.R., Fountain, T., So, E., Cohen-Gadol, A., Lee, K.H., Worrell, G.A., 2008. Phase I trial: safety and feasibility of intracranial electroencephalography using hybrid subdural electrodes containing macro- and microelectrode arrays. Neurosurg. Focus 25 (3).

Wang, M., Song, Z., 2010. Guidelines for the placement of fiducial points in image-guided neurosurgery. Int. J. Med. Robot. 6, 142–149 (December 2009).

Wellmer, J., von Oertzen, J., Schaller, C., Urbach, H., König, R., Widman, G., Van Roost, D., Elger, C.E., 2002. Digital photography and 3D MRI-based multimodal imaging for individualized planning of resective neocortical epilepsy surgery. Epilepsia 43 (12), 1543–1550.

West, J., Fitzpatrick, J.M., Wang, M.Y., Dawant, B.M., Maurer, C.R., Kessler, R.M., Maciunas, R.J., Barillot, C., Lemoine, D., Collignon, A., Maes, F., Suetens, P., Vandermeulen, D., van den Elsen, P.A., Napel, S., Sumanaweera, T.S., Harkness, B., Hemler, P.F., Hill, D.L., Hawkes, D.J., Studholme, C., Maintz, J.B., Viergever, M.A., Malandain, G., Woods, R.P., 1996. Comparison and evaluation of retrospective intermodality brain image registration techniques. J. Comput. Assist. Tomogr. 21 (4), 554–566.

Winkler, P.A., Vollmar, C., Krishnan, K.G., Pfluger, T., Brückmann, H., Noachtar, S., 2000. Usefulness of 3-D reconstructed images of the human cerebral cortex for localization of subdural electrodes in epilepsy surgery. Epilepsy Res. 41 (2), 169–178.

Woerdeman, P., Willems, P.W., Noordmans, H.J., Tulleken, C.F., van der Sprenkel, J.W.B., 2007. Application accuracy in frameless image-guided neurosurgery: a comparison study of three patient-to-image registration methods. J. Neurosurg. 106 (6), 1012–1016.

Yang, A.I., Wang, X., Doyle, W.K., Halgren, E., Carlson, C., Belcher, T.L., Cash, S.S., Devinsky, O., Thesen, T., 2012. Localization of dense intracranial electrode arrays using magnetic resonance imaging. NeuroImage 63 (1), 157–165.

Yuan, J., Chen, Y., Hirsch, E., 2012. Intracranial electrodes in the presurgical evaluation of epilepsy. Neurol. Sci. 33 (4), 723–729.